Journal of Pathology
J Pathol 2013; **229:** 477–485
Published online in Wiley Online Library
(wileyonlinelibrary.com) DOI: 10.1002/path.4136

ORIGINAL PAPER

From chaos to split-ups – SHG microscopy reveals a specific remodelling mechanism in ageing dystrophic muscle

Andreas Buttgereit,[1]* Cornelia Weber,[2] Christoph S Garbe[3] and Oliver Friedrich[1]

[1] *Institute of Medical Biotechnology, Friedrich-Alexander-University, Erlangen-Nuremberg, Germany*
[2] *Medical Biophysics, Institute of Physiology and Pathophysiology, University of Heidelberg, Germany*
[3] *Image Processing and Modelling, Interdisciplinary Centre for Scientific Computing, University of Heidelberg, Germany*

**Correspondence to: A Buttgereit, Institute of Medical Biotechnology, Friedrich-Alexander-University, Erlangen-Nuremberg, Paul-Gordan-Strasse 3, Erlangen 90152, Germany. e-mail: Andreas.Buttgereit@mbt.uni-erlangen.de*

Abstract

Duchenne muscular dystrophy (DMD) is a common inherited muscle disease showing chronic inflammation and progressive muscle weakness. Absent dystrophin renders sarcolemma more Ca^{2+}-permeable, disturbs signalling and triggers inflammation. Sustained degeneration/regeneration cycles render muscle cytoarchitecture susceptible to remodelling. Quantitative morphometry was introduced in living cells using second-harmonic generation (SHG) microscopy of myosin. As the time course of cellular remodelling is not known, we used SHG microscopy in mdx muscle fibres over a wide age range for three-dimensional (3D) rendering and detection of verniers and cosine angle sums (CASs). Wild-type (wt) and transgenic mini-dystrophin mice (MinD) were also studied. Vernier densities (VDs) declined in wt and MinD fibres until adulthood, while in mdx fibres, VDs remained significantly elevated during the life span. CAS values were close to unity in adult wt and MinD fibres, in agreement with tight regular myofibril orientation, while always smaller in mdx fibres. Using SHG 3D morphometry, we identified two types of altered ultrastructure: branched fibres and a novel, previously undetected 'chaotic' fibre type, both of which can be classified by distinct CAS and VD combinations. We present a novel model of tissue remodelling in dystrophic progression with age that involves the transition from normal to chaotic to branched fibres. Our model predicts a ~50% contribution of altered cytoarchitecture to progressive force loss with age. We also provide an improved automated image algorithm that is suitable for future ageing studies in human myopathies.

Keywords: muscular dystrophy; microarchitecture; second harmonic generation; cosine angle sum; vernier

Received 25 July 2012; Revised 10 October 2012; Accepted 12 October 2012

No conflicts of interest were declared.

Introduction

Duchenne muscular dystrophy (DMD) is the most common X-linked inherited muscle disorder that is associated with progressive muscle wasting and weakness. The causes of DMD are several mutations in the dystrophin gene that encodes for the 427 kDa isoform of dystrophin [1]. The complete absence of this cytoskeletal protein has also been shown to affect intracellular calcium homeostasis [2–6] and activity of ion channels [7]. In particular, membrane permeability towards Ca^{2+} ions has been consistently found increased; however, whether this is mostly because of contraction- or stretch-induced temporary membrane tears [8] or due to specific aberrant Ca^{2+}selective channel activities [9] is still an ongoing debate [10].

Dystrophic muscle fibres undergo continuous degeneration/regeneration cycles starting from about 4–8 weeks in mdx mice [11], with age-dependent changes in cell structure [11–14] and microarchitecture [15]. Some of the macroscopic features seen during this chronic remodelling are fibrosis, loss of muscle tissue [16] and branched fibres at the single-fibre level [13]. The appearance of branched fibres in mdx muscle shows a clear age dependence that is associated with progressive weakness [12]. Recent studies have shown that those branch points in single fibres represent a substrate for increased mechanical susceptibility towards fibre ruptures [17]. Although it has long been thought that those morphological alterations are a primary consequence of the lack of dystrophin in mdx muscle, recent models have started to suggest that the remodelling at the single-fibre level should be regarded more as a direct consequence of chronic inflammation, secondary to the increased Ca^{2+} permeability of dystrophic muscle but not directly related to absence of dystrophin [18]. Inflammation is maintained during life in dystrophic muscle [19].

Although branched fibres are an overall macroscopic parameter to assess the degree of muscle remodelling, they do not provide more insights into the alterations

present already at the subcellular architecture level. In particular, the time course of the subcellular remodelling process during ageing in mdx muscle is not known. The definition of subcellular, typical deviations from normal myofibrillar and sarcomere geometry would, therefore, be of high value to monitor progressive remodelling and correlate it to force loss, as well as to judge progression, remission or therapeutic efficiencies.

The visualization of myosin by non-linear second-harmonic generation (SHG) microscopy [20,21] has introduced a high-end imaging technology tool to study the microarchitecture in intact muscle fibres [15,22] and whole tissues [23], even in dynamic systems [24]. It is evident that the positioning and orientation of adjacent sarcomeres, as well as the lattice built by adjacent myofibrils, has significant influence on the strength of force of muscle fibres, ie misorientations from myofibrils could account for force loss in mdx fibres. From the initial coarse descriptions, eg 'wavy patterns' of myofibrillar streaks in very young mdx muscles [25], the combination of SHG imaging with image processing and pattern recognition has tremendously improved the quality of screening strategies for dystrophic cytoarchitecture. Since we have recently introduced (a) cosine angle sums (CAS) as a measure for force vector variance within a myofibre (and therefore, a measure for overall force output) and (b) 'vernier' counts as local deviations from perfectly alternating sarcomere patterns (appearing as Y-shaped structures) [15,23], we now followed the hypothesis that these parameters were suitable for monitoring disease progression in mdx muscle with age. For this purpose, we investigated hundreds of single intact fibres from wild-type (wt), dystrophic mdx and transgenic Δex 17–48 mini-dystrophin (MinD)-expressing mice [26] to present an exhaustive quantitative morphometric description of cellular alterations during the whole life spans of the animals.

Materials and methods

Single-fibre preparation, SHG-imaging and statistical analysis

For details regarding the materials and methods used in this study, see Supplementary material (Supplementary materials and methods).

Image processing and automated analysis tool

3D reconstruction was performed using the 3D-Viewer plug-in in the image analysis package Fiji, based on ImageJ. Our automated analysis tool is an image-processing algorithm in the MATLAB environment (MathWorks, Natick, MA, USA) based on boundary tensor [27]. Details and parameters used in the algorithm are described in [15,23], with some novel modifications. Deviations from the sarcomere pattern appear as Y-like structures ('verniers'). The automated tool determines the number of verniers as a function of scanned muscle fibre area. In contrast to [15], this density of verniers [VD; normalized number of verniers/100 μm^2 (#/100 μm^2)] is a function of area and not of volume throughout this study. The advantage of this presentation is that results determined in this way are independent of the distance between slices and can be compared to measurements that do not cover 3D analysis (eg thin cryosections). However, to further add robustness to the automated analysis, it was necessary to implement a cut-off criterion for the inclusion of individual slices in the overall $\overline{VD}$ count for all fibres within a genotype. It is evident that a gradient-based filter operation may introduce vast false-positive detection errors within the first slices at the border images of single fibres [23]. Therefore, to exclude a contribution from false-positive counts in the statistics, only optical sections with a dynamic fibre area cut-off were considered, which excluded slices at the edges of the fibres. The remaining slices corresponded to approximately 90% of the slices within a given fibre volume (this criterion mainly affects the statistics used in Figures 3 and 4). Another, recently used, definition of vernier density [15] used a definition that weighted the contribution of verniers counted within a single fibre volume, as given by:

$$\overline{VD} = \frac{\sum_i a_i VD_i}{\sum_i a_i} = \frac{\sum_i a_i VD_i}{A}$$

where a_i is the area of fibre/slice and $A = \Sigma_i\, a_i$ is the total area. This vernier density allows comparison between individual fibres and is suitable for a smaller number of fibres measured. It eliminates false-positive contributions at the fibre borders by the small values of a_i in those slices. This definition is used, for example, to compare the single fibres shown in Figure 1. For the statistics, we chose the above-mentioned definition over the latter because this provided us with a larger number of slices from a lower number of fibres, yet sufficient to establish a vernier density distribution function, as given in Figure 4. From the vernier density distributions, appropriate distribution models could then be applied (here, Rayleigh functions; see Results).

In addition, the automated image processing tool calculates the cosine angle sum (CAS):

$$CAS = \frac{1}{|\Omega|}\sum_{(x,y)\epsilon\Omega} \cos\left\{\Phi\,(x,y) - \text{median}\left[\Phi\,(x,y)\right]\right\}$$

where $|\Omega|$ is the number of pixels that represent the surface of the fibre, $\Phi(x,y)$ is the local direction and median $[\Phi(x,y)]$ is, in extension of [15,23], the main direction of fibres. For a perfectly linear parallel pattern, $CAS = 1$ and $CAS = 0$ for perpendicular structures; Ω is the fibre area of all slices of a whole z-stack, which implies that CAS is already the weighted mean.

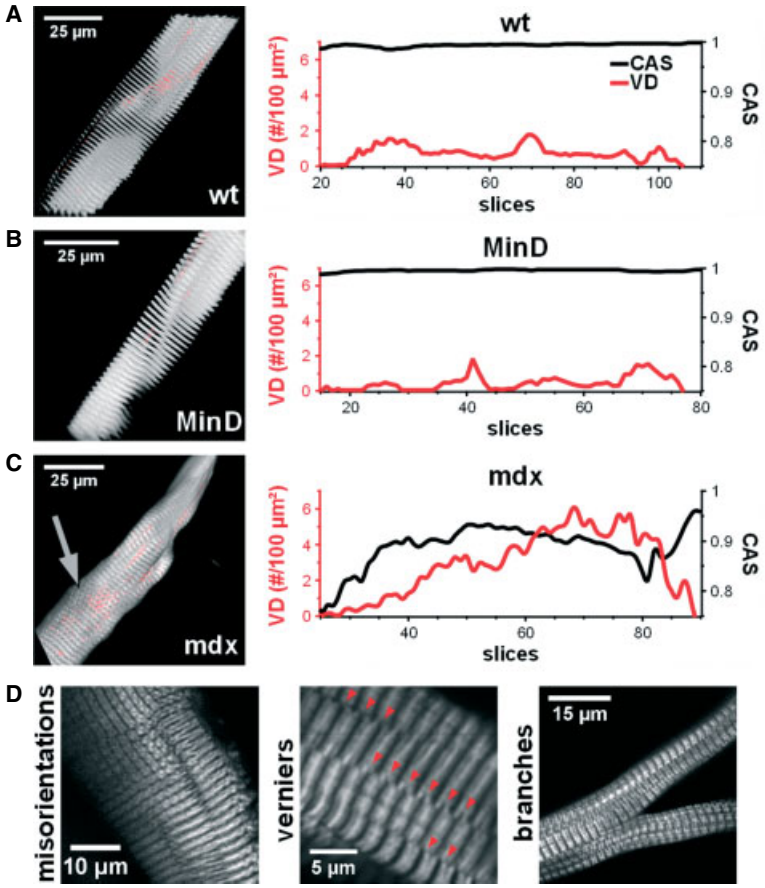

Figure 1. 3D reconstructions from SHG image stacks (grey) and detected verniers (red) in single fibres (left) from adult (5–7 months) wt (A), MinD (B) and mdx mice (C), as well as diagrams of fibre area-normalized vernier counts (red, VD) and CAS (black) through the z-stack (right). Wt and MinD fibres show an even pattern with low VD. The sarcomere pattern in mdx fibres can even appear perpendicular to the actual main direction (grey arrow) and leads to decreasing CAS values. The level of VD in wt and MinD fibres is usually low ($< 1/100\,\mu m^2$) but much increased in mdx fibres ($> 2/100\,\mu m^2$). (D) Pathological changes in the microarchitecture of mdx fibres in images of higher magnification.

Results

3D analysis of structural remodelling in single mdx fibres

To validate our automated image processing tool, we 3D-rendered complete z-stacks from individual single fibres and produced the slice-wise CAS and VD count. Figure 1 shows representative examples of single fibre sections from wt, mdx and MinD mice aged 5–10 months. Wt and MinD fibres showed an evenly spaced lattice pattern with a low index of structural alteration in microarchitecture. This is reflected by: (a) the almost unity-valued CAS through all the imaging planes within the fibres; and (b) the only sporadic counts of verniers in the two genotypes. The VDs of wt and MinD fibres rarely exceed values of $VD > 1/100\,\mu m^2$, although also in wt and MinD single fibres, locally confined increases in vernier counts may be detected in some slices; the overall slice weighted counts are $\overline{VD} < 1/100\,\mu m^2$ for the fibres shown: wt – $\overline{VD} = 0.728/100\,\mu m^2$ and MinD – $\overline{VD} = 0.424/100\,\mu m^2$. The VDs of mdx fibres were usually significantly higher. The number of verniers also robustly increased even more in the centre of the fibre. Values $> 2/100\,\mu m^2$ have been consistently observed with some slices, even resulting in values exceeding $10/100\,\mu m^2$. The VD count for the fibre shown in Figure 1 has a $\overline{VD}$ of $2.921/100\,\mu m^2$.

In mdx muscle, the appearance of fibres with macroscopic branching increases with age [13]. This process is more and more considered a secondary consequence, due to ongoing damage and regeneration, and is not specific to the lack of dystrophin *per se* [18,28]. On the other hand, it is not at all clear whether there are specific morphological alterations of cytoarchitecture prior to fibre splitting, or whether split fibres develop from a normal morphological stage. The first process would suggest a gradual remodelling of sarcomeres and myofibrils within one fibre trunk up to a 'tipping point', from which subsequent rounds of regeneration would then proceed into a split syncytium. As a first-ever approach to this question, we determined fibre morphology through several age bins.

Figure 2 shows four examples of single mdx fibres (age $\approx$ 10 months) with typical morphological changes in ultrastructure. One type of morphology is represented by fibre splitting (see Supplementary

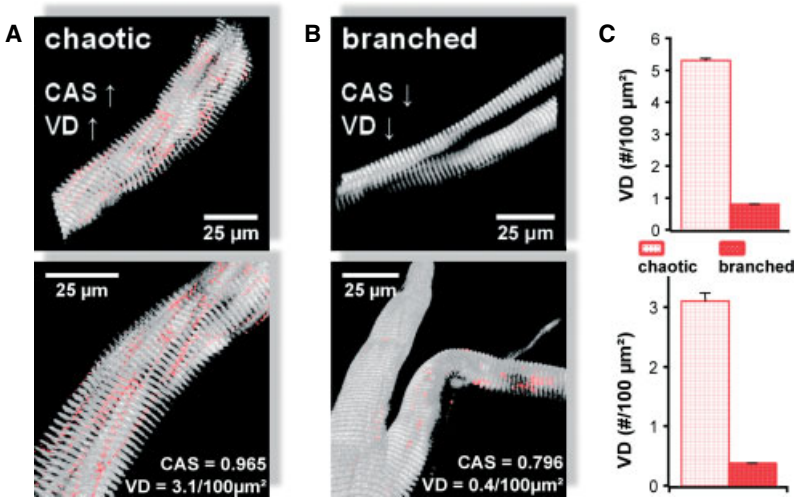

Figure 2. Two different types of micro-architectural phenotype: (A) the chaotic type is characterized by a high VD (red) and CAS; (B) within the branched type, bundles of myofibrils separate to build distinct arms of the syncytium continuous with the main fibre trunk. The other areas of the fibre may often show only minimal alteration; as a result, VD and CAS are low. (C) Comparison of VD from both types; the VD of the branched type is at the level of healthy muscle fibres.

material, Video S1). This kind of abnormality is macroscopically distinctive and also presents with CAS values of < 0.9. However, the $\overline{VD}$ count is more comparable to healthy wt fibres; $\overline{VD} = 0.792/100\,\mu m^2$ and $\overline{VD} = 0.383/100\,\mu m^2$ for the fibres shown in Figure 2B (CAS values for fibres shown, 0.967 and 0.796). The reason is that in the centre of the mdx fibre the vernier count is highest but, due to the splitting of the fibre, the centre is now the periphery of two or more branches. Thus, in these smaller fibres, the pattern of sarcomeres is similar to that in healthy muscle fibres.

Apart from the branched type with a low CAS and a low VD number, a second mdx type can be distinguished, which we call 'chaotic' (see Supplementary material, Video S2). This chaotic fibre type is characterized by a high level of $\overline{VD}$ and CAS (for the fibres shown in Figure 2A, CAS = 0.885 and CAS = 0.965, $\overline{VD} = 5.303/100\,\mu m^2$ and $\overline{VD} = 3.096/100\,\mu m^2$).

A third type is the 'wt-like'-type, which has the same pattern regarding CAS and $\overline{VD}$ (ie CAS > 0.95, $\overline{VD} < 1/100\,\mu m^2$) (see Supplementary material, Video S3).

Based on our single-fibre bins, we obtained a steady increase of branched fibres (2–4 weeks, 2%; 2–3 months, 10%; 5–7 months, 22%; 10–12 months, 32%; see also Figure 4G). Because of the fibrosis of mdx muscle, in the age group 20–24 months single fibre preparation was very difficult. Therefore, we could count only 36 muscle fibres and obtained 19% branched fibres; the percentages of chaotic and 'wt-like' types decreased accordingly.

Age-dependent morphometry of the remodelling process in single mdx fibres compared to wt and MinD fibres

Quantitative morphometry using SHG microscopy allows quantifying micro-architectural damage and remodelling. In that regard, the future selection of potential appropriate therapies might strongly depend on classification scales, eg regarding measures to determine the severity of the disease at the tissue level, as well as to provide a tool for monitoring. With our automated tool, we next quantified the age-dependent trend of micro-architectural damage in mdx muscle. Figure 3 shows box-plot diagrams of CAS and VD of wt, MinD and mdx muscle fibres from mice aged 2–4 weeks, 2–3, 5–7, 10–12 and 20–24 months.

In muscle fibres from adult wt and MinD mice, we found nearly perfectly regular linear patterns from the age groups 5–7 months or older. The CAS values in these fibres were distributed in a small interval close to unity. In the corresponding mdx muscle age groups, however, CAS values fluctuated substantially. This large scatter is explained by the two types of micro-architectural damage in mdx fibres, 'branched', and 'chaotic', resulting in a skewed, non-normal data distribution. The VD data have similar behaviour in the time course as CAS, although MinD fibres seemed to have larger VD values at very young ages (2–4 weeks), followed by lower values in both wt and mdx fibres at 2–3 months ($p < 0.01$). Since the VD values also failed for normality testing, another description of the data is needed. A good approach is provided by the Rayleigh-distribution in its modified form:

$$f(x) = \frac{A}{\sigma^2} x e^{\left\{-\frac{x^2}{2\sigma^2}\right\}}$$

where σ is the maximum of distribution, ie its most probable value. The parameter A is a arbitrary scaling parameter.

Figure 4 shows the advantage of using the Rayleigh distribution description of the VD data. Figure 4A–C shows that the distribution at age 5–7 months for wt, MinD and mdx fibres is single-peaked. The peak for mdx fibres is shifted towards larger values as compared

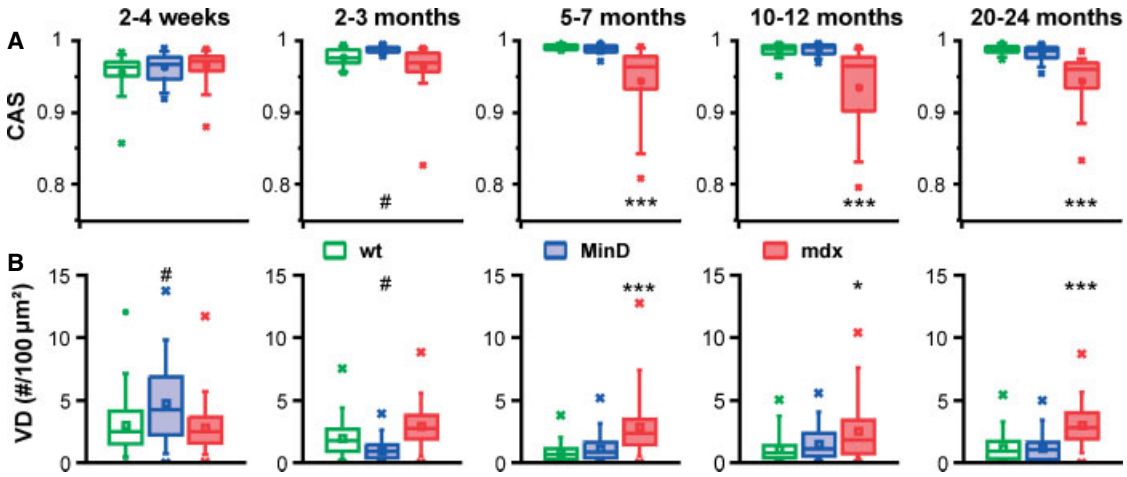

Figure 3. Boxplot diagrams (×, min, max; whisker, 5–95%; box, 25–75%; band, median; square, mean) of CAS (A) and VD (B) for different age groups. CAS values were close to unity in adult wt and MinD fibres but somewhat smaller in all muscle fibres in the age group 2–4 weeks. In adult mdx fibres, CAS values were always smaller than in the other groups. With age, VD declines in wt and MinD fibres until adulthood and stabilizes at around 5 months. In contrast, VD remained significantly elevated during the whole life span in mdx fibres. U-test, mdx versus wt/MinD, $^{*}p < 0.05$, $^{***}p < 0.01$; MinD versus wt/mdx, $^{\#}p < 0.01$.

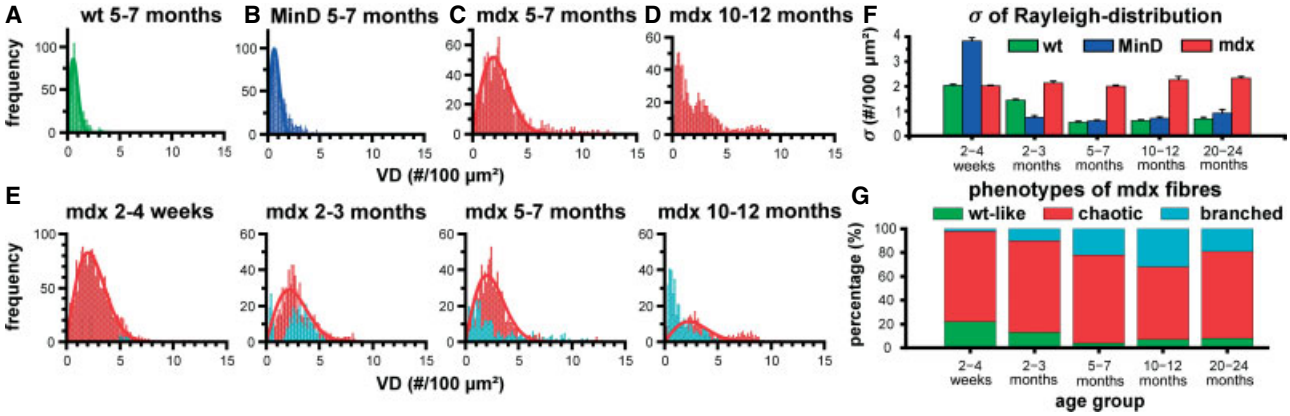

Figure 4. Histogram analysis of VD in the age group 5–7 months from wt (A), MinD (B) and mdx (C) fibres, as well as from mdx fibres from 10–12 month-old mice (D). The transformation of box–blot in a statistical histogram results in a Rayleigh distribution that was used to obtain the fits. (D) In the age group 10–12 months there are two maxima for VD in the mdx mice, while there is only one maximum for younger mdx mice and the other genotypes, irrespective of age. The first maximum, with small, ie more 'wt-like' values, corresponds to muscle fibres of the branched type; the second maximum with higher values to muscle fibres of the chaotic type. (E) Representation of both subpopulation distributions with age in all mdx fibres analysed. (F) Maximum σ of Rayleigh fit as a function of age group; the values in adult mdx mice are significantly increased and remain elevated, ie at the level of very young mice. VDs in very young MinD mice are transiently at highest values. (G) Relative weight of the three phenotypes of mdx muscle fibres as a function of age.

to the wt and MinD fibres. This changes in the older age group (10–12 months; Figure 4D), where, for mdx fibres, a distinct two-peaked distribution becomes apparent, with one peak in the range of VD counts similar to the wt and MinD, and a second peak with higher VD counts similar to the peak found in fibres from younger mdx mice. This reflects the separation into branched and chaotic mdx fibres with age. This separation is shown in Figure 4E, where the subpopulations of chaotic (red bars) and branched (cyan bars) fibres are shown. At young ages, ie before the dystrophic onset (2–4 weeks), there are hardly any branched fibres detected. Their percentage strongly increases with age, as does their VD pattern movement towards low values indicative of a 'wt-like' VD distribution, despite their branching. Since the vernier density remains fairly constant with age (Figure 4F), this is a strong indicator that the branched fibres may develop from the chaotic ones (see Discussion).

In wt and MinD fibres, σ of VD is large for very young ages, ie even larger for MinD fibres over mdx and wt fibres, but declines to a minimum value in the age group 5–7 months ($\sigma \sim 0.5/100\,\mu m^2$). In contrast, the values of VD σ in mdx fibres are constantly elevated ($\sigma \sim 2/100\,\mu m^2$). It is interesting to note that in the old-age group 20–24 months, the structural damage in the branched fibres seems to have become much higher, such that the number of verniers also substantially increases. Since at the same time the number of branched fibres is also somewhat decreased, the result was that the two peaks fused again. This fact is also visible in the boxplot diagrams.

Discussion

In clinical and preclinical studies, there is a growing interest for new diagnostics and monitoring tools to assess the severity of acquired and inherited myopathies, as well as the efficiency for treatment regimes: quantitative morphometry of microarchitecture of skeletal muscle using non-linear microscopy is a strong candidate for such a tool.

Apart from pathological processes, such as trauma and scarring [28], muscle differentiation [29], growth, exercise and regeneration [30] also substantially alter tissue and fibre architecture. The fusion of satellite cells with muscle fibres during repair processes and the synthesis of new myofilaments temporarily induce a local deviation from the normal striation pattern, which can be restored in time by regulatory processes. In normal differentiated adult muscle, as well as in muscle following complete regeneration after minor injury, most fibres show a perfectly aligned orientation pattern, ie minimal damage in healthy muscles can be completely repaired [31].

In muscular dystrophy, the occurrence frequency of muscle damage is already much higher under normal usage conditions and mostly under stretched contractions [7,17]. Although the absence of dystrophin is considered to be a trigger for impaired calcium regulation [32] and aberrant mechanotransduction [5,33], ongoing remodelling is probably more a secondary consequence of ongoing degeneration/regeneration cycles [34] and sustained inflammation [18]. Because muscle only has a limited regenerative capacity, the regenerative potential of satellite cells in dystrophic muscles decreases with age [35]. Concomitantly, the number of incompletely regenerated, and thus morphologically abnormal, muscle fibres also increases with age in mdx mice [13]. During the course of the disease, specific force declines in mdx muscles [14,36] and it is probable that this is, to a large extent, the consequence of tissue remodelling, ie fibres with deviations in their force vectors following ultrastructural remodelling [12,15].

Age-dependent monitoring of muscle fibre remodelling in mdx mice

Our improved combined SHG microscopy and image-processing approach provides new insights into the cellular sterical architecture during chronic remodelling in muscular dystrophy. The cosine of this angle may be considered as a measure for the theoretical percentage of power output. Summing over all sarcomeres, this yields a maximum power fraction. The results clearly show that the CAS may explain, at least in part, the progression of muscle weakness in mdx fibres that is related to contractile apparatus geometry when compared to wt mice. On average, this structure-related weakness may account for ~10% in fibres from aged mdx mice (Figure 3). This is somewhat lower than the values given in skinned fibre isometric force studies on the whole age range of muscle fibres that documented a power loss of 20–30% [36]. The power output of a muscle fibre is not only the result of sarcomere and myofibrillar geometry but also depends on the temporal activation profiles amongst sarcomeres. A resulting myofibrillar force vector is determined by *activation kinetics* and *direction*. The synchronized *activation* of all myofibrils within a fibre volume is governed by simultaneous excitation spread and ec-coupling, whereas *direction* is mainly determined by the microarchitecture of the muscle fibre. Both characteristics are disturbed in dystrophic muscle [17,18] when there are various branches present in one fibre. In unbranched fibres from young mdx mice, surface and t-tubular action potential properties were unchanged compared to wt fibres [37]. Thus, in those younger age groups where unbranched fibres still predominate, the imbalance in Ca^{2+} homeostasis with increased membrane permeability might be considered as one of the driving forces to sustain chronic inflammation, amongst other factors [10]. However, our study clearly shows that also in those early stages, alterations of myofibrillar geometry can be determined that have not been previously detected. Those detections and classifications are well reflected by the CAS values of fibres.

Another landmark of altered ultrastructure in dystrophic muscle are verniers that also have been reported in muscle of desmin knockout mice [38] and weight-lift rat models [30]. The results from desmin-deficient mice show the elementary role of desmin in cell architecture and force transmission [39]. The same microscopic appearance of verniers in desmin- and dystrophin-deficient muscle suggests that lateral force transmission is also disturbed in dystrophic muscle fibres [40]. Although the localization of desmin and dystrophin may have different implications for the lateral force transmission within the fibre and towards the extracellular matrix, it is surprising that the ultrastructural alterations (ie presence of verniers in the middle of a fibre volume) are very similar. It can be speculated that somehow, also for dystrophic muscle, the power of single myofibrils is not correctly transmitted laterally to the extracellular matrix. In fact, in overloaded fibres, damaged z-disks have been observed [41]. Therefore the decrease of z-disk connection with age is another reason for the progressive weakness of muscles in mdx mice. It certainly correlates with the degree of regeneration, since similar changes in ultrastructure are observed in attempts of regeneration from chronic damage [28,31]. Such shifts in the myofibrillar lattice that underlie 'verniers' can easily be estimated by our tool (ie the parameter *VD*), the number of which may also relate to the degree of cellular maturation or remodelling. For instance, MinD fibres showed higher VD levels at very young ages (2–4 weeks) and then very low VD values compared to both wt and mdx fibres (2–3 months), which may point towards a faster maturation process in this genotype that still has to be confirmed experimentally.

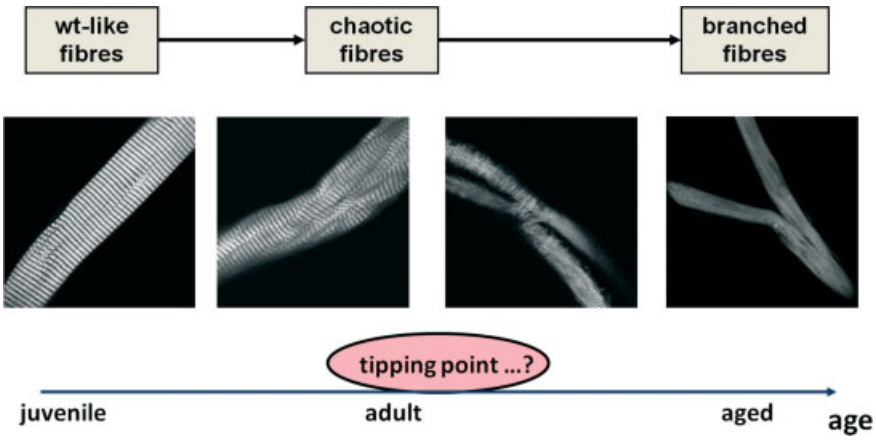

Figure 5. Suggested scenario for the transformation of dystrophic muscle fibres. The regeneration phase in dystrophic muscle fibres leads to deformations in the ultrastructure. From a wt-like-fibre is formed a chaotic fibre. The mechanical destabilization of the muscle fibre results finally in branching.

One of the novel findings of our study was the presence of two distinct abnormal cell architectures: a branched type that has been extensively studied previously [17], and a chaotic fibre type that has not been described before. This latter type was characterized by a high VD but also a high CAS value, which is different from the branched type, which had a low VD, more similar to wt fibres, but a low CAS value. Most interestingly, while the branched type clearly increased in frequency with age, the percentage of chaotic fibres decreased.

The decrease of CAS and the increase of VD of mdx fibres with age have their origin in the same two-stage process [17]. In the first stage, the altered function of ion channels and the increase of calcium in muscle fibres induce the activation of cell damage pathways. The regeneration of the fibres leads to deformations in the ultrastructure. In this phase, the number of verniers and the CAS are high; we find many fibres from the chaotic type. In the second stage, the deformations result in branching of the muscle fibres. That means that the branched fibres likely originated from the chaotic type. In this phase, the number of verniers and the CAS decrease. This view is also supported by an age-dependent comparison of the relative weight of the three fibre types in mdx fibres, where an exhaustion of wt-like fibres is found with age. A relatively constant proportion of chaotic fibres is found up to 5–7 months, after which their proportion decreases as branched fibres become more apparent (Figure 4 G).

It is well known that central nuclei are a hallmark of regenerating fibres. Also, we see that the VD is largest in its distribution within the fibres' central areas at young ages. If one would postulate that through the ongoing degeneration/regeneration cycles fibres became mechanically destabilized from within, one could potentially explain why branched fibres show decreased VD and CAS values at older age. Local membrane damage gives rise to Ca^{2+} influx and activation of inflammatory signalling cascades and ROS production [10]. Since in Duchenne muscular dystrophy local membrane repair mechanisms induced by dysferlin and mitsugumin-53 are impaired [8], a more vigorous subsequent activation of quiescent satellite cells is expected. Indeed, increased activation of satellite cells in mdx muscle has been found [42]. Once satellite cells are activated, they migrate to damage sites and the cell interior [43], where they build new myotubes to fuse into the muscle fibres. This precipitous process in dystrophic muscle may then result in the ongoing build-up of centrally located high vernier densities and the chaotic phenotype. However, through ongoing damage and remodelling, there may exist a 'tipping point' from which on further repair might destabilize the central fibre parts in a way that they simply split up and the defect is closed by enwrapping sarcolemma, leaving a branched fibre. Since the previously misaligned lattice of those adjacent myofibrils has now become separate, the verniers no longer exist in those two separate arms. As a result, VD declines and CAS increase (from similar considerations). Our results provide a strong support for this scenario (shown in Figure 5), ie an increase in branched and a decrease in chaotic fibres with age, the latter potentially also coinciding with a decrease in the regenerative potential of mdx fibres [44]. One constraint of our study is the use of larger populations of different fibres in age bins. A more direct confirmation of the aforementioned scenario would require to repetitively revisit one and the same single fibre *in vivo* over a long time period, which is currently not possible.

In conclusion, our study provides a new tool, combining SHG microscopy with automated image processing, to provide a platform for quantitative morphometry in living muscle fibres and tissue. The technological development of multiphoton endoscopy solutions has recently started to touch a new era of applicability in humans, using a minimally invasive approach [24]. In parallel with *in vivo* morphometry, suitable image database information now needs to be

generated on various human muscle diseases to correlate morphometric parameters with disease diagnostics and to monitor the severity of disease progression as well as therapy efficiency.

Acknowledgements

The authors thank RHA Fink (Heidelberg) for generous provision of laboratory space and equipment access. The study was partly funded by the Deutsche Forschungsgemeinschaft (DFG; Grant No. FR-1499/7-1 to OF). OF acknowledges ongoing support by the Erlangen Graduate School of Advanced Optical Technologies (SAOT) within the German Excellence Initiative. This study is part of a PhD thesis by AB.

Author contributions

AB and OF designed the experimental procedure; OF supervised the project; CG and OF developed the pattern recognition tool; CG and AB made further improvements and additional automation; AB and CW performed the study and verified the data; and AB analysed the data with the automated tool and worked on the statistical analysis and description. All authors wrote the manuscript.

References

1. Hoffman EP, Brown RH Jr, Kunkel LM. Dystrophin: the protein product of the Duchenne muscular dystrophy locus. *Cell* 1987; **51:** 919–928.
2. Friedrich O, Both M, Gillis JM, *et al*. Mini-dystrophin restores L-type calcium currents in skeletal muscle of transgenic mdx mice. *J Physiol* 2004; **555:** 251–265.
3. Friedrich O, von Wegner F, Chamberlain JS, *et al*. L-type Ca^{2+} channel function is linked to dystrophin expression in mammalian muscle. *PLoS One* 2008; **3:** e1762.
4. Gailly P. New aspects of calcium signaling in skeletal muscle cells: implications in Duchenne muscular dystrophy. *Biochim Biophys Acta* 2002; **1600:** 38–44.
5. Teichmann MD, Wegner FV, Fink RH, *et al*. Inhibitory control over Ca^{2+} sparks via mechanosensitive channels is disrupted in dystrophin deficient muscle but restored by mini-dystrophin expression. *PLoS One* 2008; **3:** e3644.
6. Whitehead NP, Yeung EW, Allen DG. Muscle damage in mdx (dystrophic) mice: role of calcium and reactive oxygen species. *Clin Exp Pharmacol Physiol* 2006; **33:** 657–662.
7. Yeung EW, Head SI, Allen DG. Gadolinium reduces short-term stretch-induced muscle damage in isolated mdx mouse muscle fibres. *J Physiol* 2003; **552:** 449–458.
8. Cai C, Weisleder N, Ko JK, *et al*. Membrane repair defects in muscular dystrophy are linked to altered interaction between MG53, caveolin-3, and dysferlin. *J Biol Chem* 2009; **284:** 15894–15902.
9. McCarter GC, Steinhardt RA. Increased activity of calcium leak channels caused by proteolysis near sarcolemmal ruptures. *J Membr Biol* 2000; **176:** 169–174.
10. Allen DG, Whitehead NP. Duchenne muscular dystrophy – what causes the increased membrane permeability in skeletal muscle? *Int J Biochem Cell Biol* 2011; **43:** 290–294.
11. Tanabe Y, Esaki K, Nomura T. Skeletal muscle pathology in X chromosome-linked muscular dystrophy (mdx) mouse. *Acta Neuropathol* 1986; **69:** 91–95.
12. Chan S, Head SI, Morley JW. Branched fibers in dystrophic mdx muscle are associated with a loss of force following lengthening contractions. *Am J Physiol Cell Physiol* 2007; **293:** C985–992.
13. Head SI, Williams DA, Stephenson DG. Abnormalities in structure and function of limb skeletal muscle fibres of dystrophic mdx mice. *Proc Biol Sci* 1992; **248:** 163–169.
14. Pastoret C, Sebille A. mdx mice show progressive weakness and muscle deterioration with age. *J Neurol Sci* 1995; **129:** 97–105.
15. Friedrich O, Both M, Weber C, *et al*. Microarchitecture is severely compromised but motor protein function is preserved in dystrophic mdx skeletal muscle. *Biophys J* 2010; **98:** 606–616.
16. Blake DJ, Weir A, Newey SE, *et al*. Function and genetics of dystrophin and dystrophin-related proteins in muscle. *Physiol Rev* 2002; **82:** 291–329.
17. Head SI. Branched fibres in old dystrophic mdx muscle are associated with mechanical weakening of the sarcolemma, abnormal Ca^{2+} transients and a breakdown of Ca^{2+} homeostasis during fatigue. *Exp Physiol* 2010; **95:** 641–656.
18. Chan S, Head SI. The role of branched fibres in the pathogenesis of Duchenne muscular dystrophy. *Exp Physiol* 2011; **96:** 564–571.
19. Tang Y, Reay DP, Salay MN, *et al*. Inhibition of the IKK/NF-κB pathway by *AAV* gene transfer improves muscle regeneration in older mdx mice. *Gene Ther* 2010; **17:** 1476–1483.
20. Both M, Vogel M, Friedrich O, *et al*. Second harmonic imaging of intrinsic signals in muscle fibers *in situ*. *J Biomed Opt* 2004; **9:** 882–892.
21. Plotnikov SV, Millard AC, Campagnola PJ, *et al*. Characterization of the myosin-based source for second-harmonic generation from muscle sarcomeres. *Biophys J* 2006; **90:** 693–703.
22. Ralston E, Swaim B, Czapiga M, *et al*. Detection and imaging of non-contractile inclusions and sarcomeric anomalies in skeletal muscle by second harmonic generation combined with two-photon excited fluorescence. *J Struct Biol* 2008; **162:** 500–508.
23. Garbe CS, Buttgereit A, Schurmann S, *et al*. Automated multiscale morphometry of muscle disease from second harmonic generation microscopy using tensor-based image processing. *IEEE Trans Biomed Eng* 2012; **59:** 39–44.
24. Llewellyn ME, Barretto RP, Delp SL, *et al*. Minimally invasive high-speed imaging of sarcomere contractile dynamics in mice and humans. *Nature* 2008; **454:** 784–788.
25. Plotnikov SV, Kenny AM, Walsh SJ, *et al*. Measurement of muscle disease by quantitative second-harmonic generation imaging. *J Biomed Opt* 2008; **13:** 044018.
26. Phelps SF, Hauser MA, Cole NM, *et al*. Expression of full-length and truncated dystrophin mini-genes in transgenic mdx mice. *Hum Mol Genet* 1995; **4:** 1251–1258.
27. Köthe U. Integrated edge and junction detection with the boundary tensor. In Proceedings of the 9th International Conference on Computer Vision, IEEE Computer Society, Los Alamitos, 2003; 424–431.
28. Tamaki T, Akatsuka A. Appearance of complex branched fibers following repetitive muscle trauma in normal rat skeletal muscle. *Anat Rec* 1994; **240:** 217–224.
29. Merrick D, Stadler LK, Larner D, *et al*. Muscular dystrophy begins early in embryonic development deriving from stem cell loss and disrupted skeletal muscle formation. *Dis Model Mech* 2009; **2:** 374–388.
30. Ho KW, Roy RR, Tweedle CD, *et al*. Skeletal muscle fiber splitting with weight-lifting exercise in rats. *Am J Anat* 1980; **157:** 433–440.

31. Lancut M, Godlewski P, Lis-Sochocka M, *et al*. Investigations of ultrastructure of damaged and regenerated skeletal muscle fibers. *Ann Univ Mariae Curie Sklodowska Med* 2004; **59:** 80–85.
32. DiFranco M, Woods CE, Capote J, *et al*. Dystrophic skeletal muscle fibers display alterations at the level of calcium microdomains. *Proc Natl Acad Sci USA* 2008; **105:** 14698–14703.
33. Lovering RM, Michaelson L, Ward CW. Malformed mdx myofibers have normal cytoskeletal architecture yet altered EC coupling and stress-induced Ca^{2+} signaling. *Am J Physiol Cell Physiol* 2009; **297:** C571–580.
34. Yokota T, Lu QL, Morgan JE, *et al*. Expansion of revertant fibers in dystrophic mdx muscles reflects activity of muscle precursor cells and serves as an index of muscle regeneration. *J Cell Sci* 2006; **119:** 2679–2687.
35. Blau HM, Webster C, Pavlath GK. Defective myoblasts identified in Duchenne muscular dystrophy. *Proc Natl Acad Sci USA* 1983; **80:** 4856–4860.
36. Lynch GS, Hinkle RT, Chamberlain JS, *et al*. Force and power output of fast and slow skeletal muscles from mdx mice 6–28 months old. *J Physiol* 2001; **535:** 591–600.
37. Woods CE, Novo D, DiFranco M, *et al*. Propagation in the transverse tubular system and voltage dependence of calcium release in normal and mdx mouse muscle fibres. *J Physiol* 2005; **568:** 867–880.
38. Li Z, Mericskay M, Agbulut O, *et al*. Desmin is essential for the tensile strength and integrity of myofibrils but not for myogenic commitment, differentiation, and fusion of skeletal muscle. *J Cell Biol* 1997; **139:** 129–144.
39. Paulin D, Li Z. Desmin: a major intermediate filament protein essential for the structural integrity and function of muscle. *Exp Cell Res* 2004; **301:** 1–7.
40. Ramaswamy KS, Palmer ML, van der Meulen JH, *et al*. Lateral transmission of force is impaired in skeletal muscles of dystrophic mice and very old rats. *J Physiol* 2011; **589:** 1195–1208.
41. Vaughan HS, Goldspink G. Fibre number and fibre size in a surgically overloaded muscle. *J Anat* 1979; **129:** 293–303.
42. Wozniak AC, Anderson JE. Nitric oxide dependence of satellite stem cell activation and quiescence on normal skeletal muscle fibers. *Dev Dyn* 2007; **236:** 240–250.
43. Terada M, Lan YB, Kawano F, *et al*. Myonucleus-related properties in soleus muscle fibers of mdx mice. *Cells Tissues Organs* 2010; **191:** 248–259.
44. Heslop L, Morgan JE, Partridge TA. Evidence for a myogenic stem cell that is exhausted in dystrophic muscle. *J Cell Sci* 2000; **113**(12): 2299–2308.

SUPPLEMENTARY MATERIAL ON THE INTERNET

The following supplementary material may be found in the online version of this article:

Supplementary materials and methods

Video S1. 3D reconstruction of a branched muscle fibre with two split-ups from a 3 month-old mdx mouse. This phenotype is characterized by low levels of CAS and VD

Video S2. 3D reconstruction of a chaotic muscle fibre from a 3 month-old mdx mouse. This phenotype is characterized by high levels of CAS and VD, as well as twists and tilts

Video S3. 3D reconstruction of a muscle fibre from an 11 month-old wt mouse. The regular lattice leads to a low level of VD und a normal CAS value close to unity